Applied Materials Today 19 (2020) 100597

Contents lists available at ScienceDirect

Applied Materials Today

journal homepage: www.elsevier.com/locate/apmt

Liquid metal droplet robot

Fangxia Li[a,1], Jian Shu[b,1], Leran Zhang[b,1], Nailin Yang[c], Jie Xie[b], Xiangpeng Li[a,f,*], Liang Cheng[c], Shaolong Kuang[a], Shi-Yang Tang[d,*], Shiwu Zhang[b,*], Weihua Li[d], Lining Sun[a], Dong Sun[e]

[a] Robotics and Microsystems Center, School of Mechanical and Electric Engineering, Soochow University, Suzhou, 215000, China
[b] CAS Key Laboratory of Mechanical Behavior and Design of Materials, Department of Precision Machinery and Precision Instrumentation, University of Science and Technology of China, Hefei, 230026, China
[c] Institute of Functional Nano & Soft Materials (FUNSOM), Jiangsu Key Laboratory for Carbon-Based Functional Materials and Devices, Soochow University, Suzhou, 215123, China
[d] School of Mechanical, Materials, Mechatronic and Biomedical Engineering, University of Wollongong, Wollongong, NSW 2522, Australia
[e] Department of Biomedical Engineering, City University of Hong Kong, Kowloon, Hong Kong
[f] State Key Laboratory of Applied Optics, Changchun Institute of Optics, Changchun, 130033, China

ARTICLE INFO

Article history:
Received 15 December 2019
Received in revised form 31 January 2020
Accepted 4 February 2020

Keywords:
Liquid metal
Soft robotics
EGaIn
3D actuation
Targeted drug delivery

ABSTRACT

Liquid metal (LM) droplets made from gallium-based alloys exhibit excellent biomimetic locomotion and deformation capabilities under external stimulating fields and have presented potentials in a variety of applications. However, its application in robotics is presently hampered by limited maneuverability in two-dimensional (2D) space and weak cargo carrying capacity. Here, we propose a composite liquid metal droplet robot (LMDR) which appears as a LM droplet but exhibits an extraordinary actuating performance in 3D space. The LMDR is fabricated by assembling a hollow and spherical-shaped magnetic internal framework (IF) into a LM droplet, and the IF can be disassembled from the LM droplet with the application of an external magnetic field. The maneuver of the LMDR is realized using the interplay of electric and magnetic fields, and complex actuation especially jumping to avoid obstacles, climbing steep slopes, and rotating its body to the desired posture can be achieved. The hollow IF within the LMDR has a cargo carrying capacity and we demonstrate a proof-of-concept experiment to show the transportation and controlled release of a chemical indicator using the LMDR. More importantly, an *in vitro* targeted drug delivery and therapy trial to treat breast cancer cells (4T1) with a drug loaded LMDR is also successfully performed. The demonstrated capabilities of the LMDR present a promising potential in developing future targeted drug delivery and soft robotic systems with high controllability and multi-functionalities.

1. Introduction

Liquid droplets are very simple object in everyday life but play extremely important roles for many natural phenomena [1–3]. Gallium based liquid metal (LM) droplets made from eutectic gallium-indium (EGaIn) and Galinstan (gallium-indium-tin) exhibit unique and extraordinary properties as living protoplasm. Over the years, many researchers have been trying to employ LM droplets as animated soft matter to create liquid robots that can possess complex characteristics and behaviors of living systems [4–6]. Up to now, many biomimetic phenomena and behaviors of LM droplets have been revealed, including separation and fusion [7], engulfing [8], breathing [9], locomotion [10,11] and deformation [12,13].

Locomotion of LM droplet is commonly realized by applying an external electrical potential to induce a gradient of interfacial tension on its surface within electrolytes [14]. However, the driving force generated by surface tension is weak and limits LM droplet for overcoming gravity. Thus, locomotion of LM droplets is restricted within two-dimensional space. Through coating or mixing LM with functional materials, LM droplets can be actuated using magnetic [15,16], chemical [8,17] or optical approaches [18]. However, this significantly affects the intrinsic properties and compromises the liquidity of the LM droplets.

In terms of using LM for the applications in cargo delivery, LM droplets can be designed to transport and unload drugs adhered on the oxide layer [19–21]. In addition, several investigations have employed LM droplet as actuators to create boat-like and wheel-like robots that that can realize diverse locomotion and powerful carrying capacity [22,23]. Nonetheless, entrusting LM droplets with

* Corresponding authors.
E-mail addresses: licool@suda.edu.cn (X. Li), shiyang@uow.edu.au (S.-Y. Tang), swzhang@ustc.edu.cn (S. Zhang).
[1] These authors contributed equally to this work.

https://doi.org/10.1016/j.apmt.2020.100597
2352-9407/

carrying capability *per se* without destroying its intrinsic properties remains unsolved in current studies.

Limited 3D maneuver performance and weak carrying capacity are the two major chasms between LM droplets and powerful soft living robot. In this study, we proposed an innovative composite liquid metal droplet robot (LMDR) which appears as a LM droplet but exhibits extraordinary actuating performance in 3D space. We investigated the use of the interplay of electric and magnetic fields to induce complex actuation including climbing steep slopes, jumping to avoid obstacles, and rotating its body to the desired posture. The LMDR was fabricated by engulfing a spherical-shaped magnetic internal framework (IF) into an EGaIn LM droplet. The IF is coated with copper and its inner spaces contains three cabins: *1)* the driving cabin which entrusts complex magnetic driving capabilities to the LMDR; *2)* the counterweight cabin which maintains the appropriate posture of the LMDR during motion; and *3)* the cargo cabin which entrusts the LMDR with cargo loading and releasing capability. A proof-of-concept experiment of transporting and releasing chemical pH indicator using the LMDR was performed to demonstrate its capability in realizing controlled and complex cargo-delivery applications. Finally, we conducted an *in vitro* targeted drug delivery and therapy trial to treat breast cancer cells (4T1) with a drug loaded LMDR to reveal the potentials of developing future drug delivery and therapy systems using the LMDR-based platforms.

2. Materials and methods

2.1. Materials

EGaIn alloy (75% Ga, 25% In, Sigma-Aldrich, USA) was used as the metallic liquid base. Nickel nanoparticles (diameter of 100 nm, Shanghai Yu-sui Welding Material) were chosen as the magnetic material. The phenolphthalein power (C20H14O4, FUCHEN CHEMICAL REAGENTS, China) was used as the color pH indicator. The electrolyte used in all experiments was NaOH aqueous solution (0.5 M).

The murine breast cancer 4T1 cell line used in the targeted drug delivery and therapy trial was obtained from American Type Culture Collection (ATCC). All cell culture related reagents were purchased from HyClone. The anticancer drug used in the targeted drug delivery experiment was doxorubicin (DOX) obtained from Beijing HuaFeng United Technology Co., Ltd.

2.2. Fabrication of PMMA channels

All channels used in experiments were fabricated by milling transparent polymethylmethacrylate (PMMA). The obstacle used in the jumping test was fabricated by laser-cutting a PMMA block.

2.3. Generating magnetic field and electrical potential

Magnetic field in the experiments was generated by a commercially-available cylindrical neodymium-iron-boron (NdFeB) permanent magnet (maximum magnetic flux density of 2500 Gs), a rectangle NdFeB permanent magnet (maximum magnetic flux density of 4000 Gs), and an electromagnet (P34/25, Fanke Electric Company, China). The DC voltages were provided by a DC power supply (IT6432, ITECH, China). All the electrodes were graphite electrodes.

2.4. Videos and photos

Videos were captured using a DSLR camera (5D MARK2, Canon, Japan), and the snapshots were extracted from these videos. The velocity data was obtained using a high-speed camera (HERO 5,

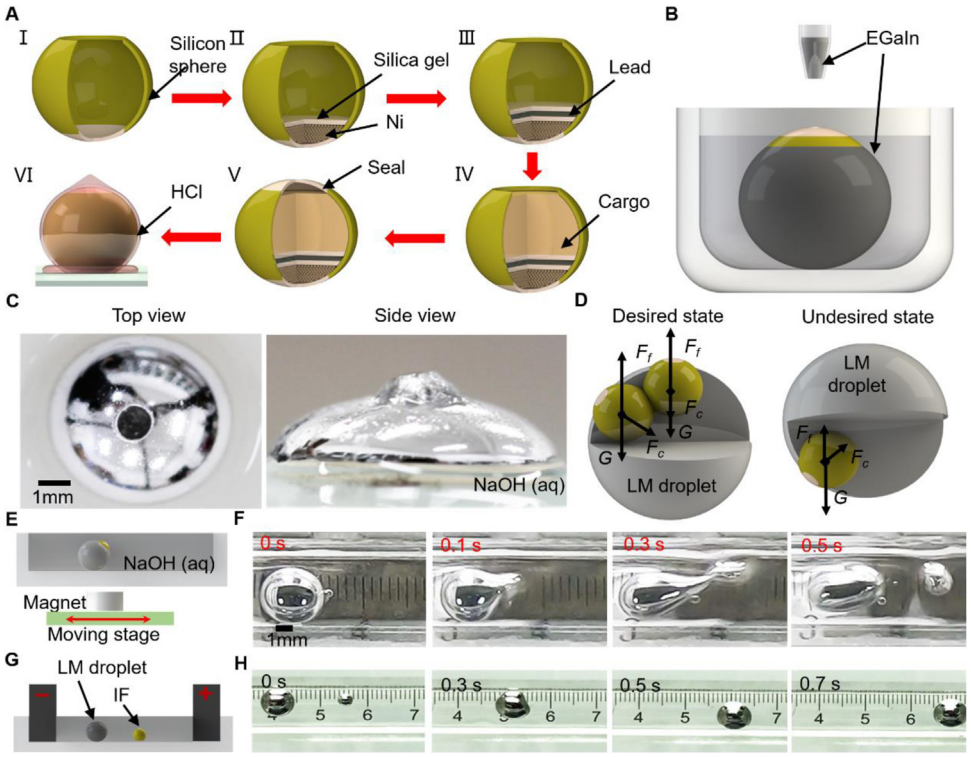

Fig. 1. Fabrication process of a LMDR. (A) Fabrication process of the IF. (B) Coating the IF with a layer of EGaIn. (C) Top and side-view images of a LMDR at the desired state. (D) Dynamics of the LMDR: the left schematic shows the desired state, and the right schematic shows the undesired state. (E) Schematic of the experimental setup, and (F) Sequential snapshots for showing the separation of the IF from the LM droplet using a magnet. (G) Schematic of the experimental setup, and (H) Sequential snapshots for showing the assembling process of the LMDR upon the application of an external electrical potential.

GoPro, USA). The confocal fluorescence images are taken by a confocal laser scanning microscope (CLSM, Zeiss Axio-Image LSM-800, Germany).

3. Results and discussion

The preparation process for producing the LMDR is illustrated in Fig. 1A-B, which can be specified as follows:

1 *IF fabrication*: We used a hollow silicon sphere coated with copper (weight of 30 mg, diameter of 3 mm) as the skeleton frame of the IF, as shown in Fig. 1A. We drilled a small opening with the diameter of 1 mm on the sphere for filling materials. The inner space of the sphere contains three individual functional cabins. The *driving cabin* is located at the bottom of the sphere. It was made by filling 25 mg of ferro-magnetic materials (Ni nanoparticles, 100 nm) and sealed with a thin layer of silica gel. With the presence of the driving cabin, the LMDR can be maneuvered using an external magnetic field. The *counterweight cabin* is located at the middle part of the sphere. Pre-calculated lead particles were filled in the sphere and sealed with a layer of silica gel. The lead particles in the counterweight cabin can balance the loading distribution of the IF to keep appropriate posture of the LMDR during motion. The *cargo cabin* is located on the top of the sphere. After the cargo is loaded, the opening can be sealed with stimuli-responsive materials according to the desired cargo release approaches.

2 *LMDR fabrication*: We first treated the IF with 500 μL HCl (37% wt) and then immerse the IF into a tube filled with EGaIn (volume of 100 μL) for 15 min, as illustrated in Fig. 1B. The surface of the IF can be uniformly coated with a thin layer of EGaIn, indicating that the IF can be easily wrapped into a LM droplet. Finally, the LM coated IF was transferred into an EGaIn droplet (volume of 30 μL) to complete the fabrication process of the LMDR.

The LMDR can exhibit two states during motion by adjusting the average density of the IF, which can be achieved by configuring the amount of lead particles filled in the counterweight cabin (see Supplementary Information S1). When the average density of the IF is smaller than that of LM (6.55 mg/μL), the IF can float on the top of the LM droplet and we can see the exposed sealing material of the IF, as shown in Fig. 1C. We termed this state as the desired state since the LMDR exhibits a better performance in actuation. In such a state, the inertia forces or external disturbances induced during motion may pulled the IF away from the top of LM droplet, however, the IF can return to the top of the LM droplet rapidly. In contrast, when the average density of the IF is equal or larger than that of LM, the IF may sink to the bottom of the droplet and touch the substrate during motion. Such a situation may hinder the flexible maneuvers of the LMDR, and we therefore termed this state as the undesired state. The underlying mechanism for the two states of LDMR lies in the dynamic equilibrium of three forces act on the IF (Fig. 1D): the gravity G, the buoyant force F_f, and the capillary force F_c that always points to the center of the LM droplet. The dynamics of LDMR is formulated in Fig. S1, Supplementary Information S2.

The LMDR can be assembled within a sodium hydroxide (NaOH) solution by combining the IF and a LM droplet upon the application of an external electrical potential; also, the IF and the LM droplet can be separated using a magnet. Fig. 1E-F show the separating process of a LMDR using a magnet. A LMDR (the volume of the LM droplet is 100 μL) was placed into a straight channel (length of 200 mm, width of 10 mm, and height of 12 mm) filled with NaOH solution (0.5 M), where a magnet (B = 2500 Gs) was positioned underneath the channel and fixed on a moving stage (Fig. 1E). The moving stage can actuate to pull the IF with a pre-set constant acceleration. Fig. 1F shows the time lapse images of the disassembling process after accelerating the magnet under the LMDR, in which we can clearly see the separation of the IF from the LM droplet. The underlying mechanism of the disassembling process is explained in Fig. S2, Supplementary Information S3. Fig. 1G-H show the assembling process of a LMDR by applying an electrical potential. Upon the application of a 15 V DC voltage to the electrodes located at the both ends of the channel, the LM droplet can move toward the IF and engulf the IF to form a LMDR. After assembly, the LMDR can continuously move towards the anode, which is similar to the case of a bare LM droplet [24].

We next performed a series of experiments to investigate the relationship between the carrying capacity and the actuating performance of the LMDR. LMDRs with different volume and density ratios of IF to LM were placed into a straight channel (length of 150,

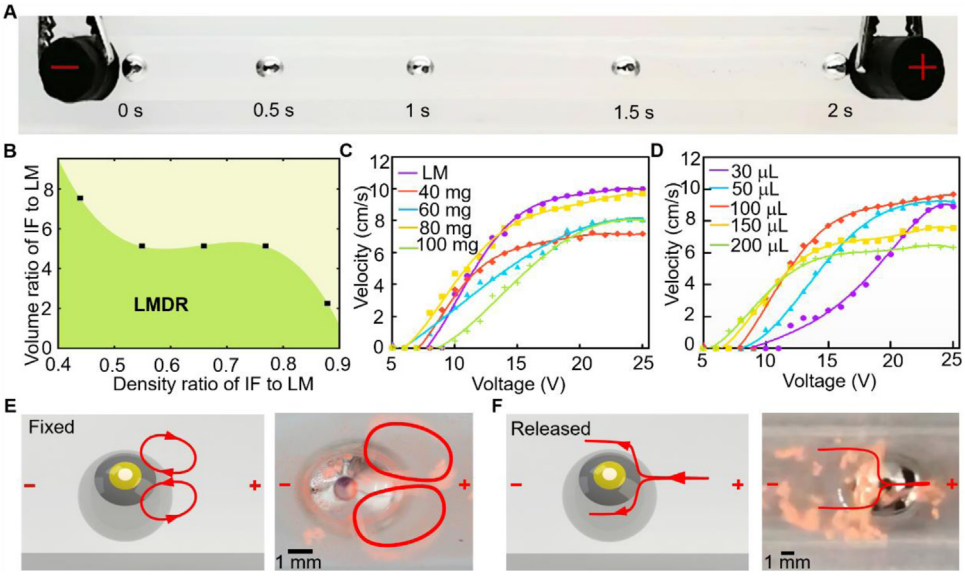

Fig. 2. Investigating the carrying capacity and electrical actuating performance of the LMDR. (A) Snapshots of the electrical locomotion of a LMDR in a straight channel. (B) Constraints for allowing the LMDR to actuate upon the application of an electrical potential. (C) Electrical actuating performance of LMDRs fabricated with a fixed volume of LM (100 μL) but with IFs of different weights. (D) Electrical actuating performance of LMDRs with a fixed weight of IF (60 mg) and different volumes of LM. (E) Schematic and actual image showing the position of the IF when the LMDR is fixed. (F) Schematic and actual image showing the position of the IF when the LMDR is released.

width of 10 mm) filled with NaOH solution (0.5 M). When applying a DC voltage between the two electrodes fixed at the two ends of the channel, LMDRs with proper volume and density ratios are expected to move toward the anode similar to the case of a bare LM droplet [24], as shown in Fig. 2A. However, there exists a minimum required volume of LM and a maximum density of the IF for allowing the LMDR to actuate upon the application of a DC voltage (i.e. the LMDR is in the desired state given in Fig. 1D), as illustrated in Fig. 2B. The area above the curve means that the LMDR cannot be actuated. When the volume of the LM droplet is set constant, a heavier IF can increase the frictional force between LMDR and the channel and therefore, compromise the actuating performance. On the other hand, when the density of the IF is set constant, a larger volume of the LM droplet can generate a larger driving force for enhancing the actuating performance.

We investigated the electrical actuating performance of LMDRs fabricated with a fixed volume of LM (100 μL) but with IFs of different weights, which is characterized by obtaining their velocity-voltage relationship, as shown in Fig. 2C and Tab. 1 of Supplementary Information S4. Similar to the case of a bare LM (EGaIn) droplet, the velocity of all LMDRs increases with the increase in voltage until it reaches a saturation point at ~20 V, after which the velocity does not significantly increase. Interestingly, the velocity of the LMDRs increases until the weight of the IF is above 80 mg. The average density of the IF with a weight less than 80 mg is much lower than that of LM, as such, most part of the IF is exposed outside the LM droplet in a LMDR. The exposed surface of the IF could bring extra hydrodynamic friction, and this results in the decrease in velocity of the LMDR. However, the increase in frictional force between the LMDR and the substrate can also cause the decrease in velocity if the weight of IF exceeds 80 mg (Fig. 2C). We can, therefore, conclude from this experiment that the optimal weight of the IF is between 60–80 mg. However, to maximize the space of the cargo cabin for loading drugs, we chose to use an IF with the weight of 60 mg for the rest of the experiments. We further studied the electrical actuating performance of LMDRs with different volumes of LM, as shown in Fig. 2D and Tab. 2 of Supplementary Information S4. We can see that it requires less voltage to start actuating a LMDR with a larger volume of LM. Interestingly, we observed that the saturation voltage is lower for a LMDR with a larger volume of LM. This can be attributed to the increased friction between the LMDRs and the channel. Also, Fig. 2D clearly shows that the LMDR with a LM

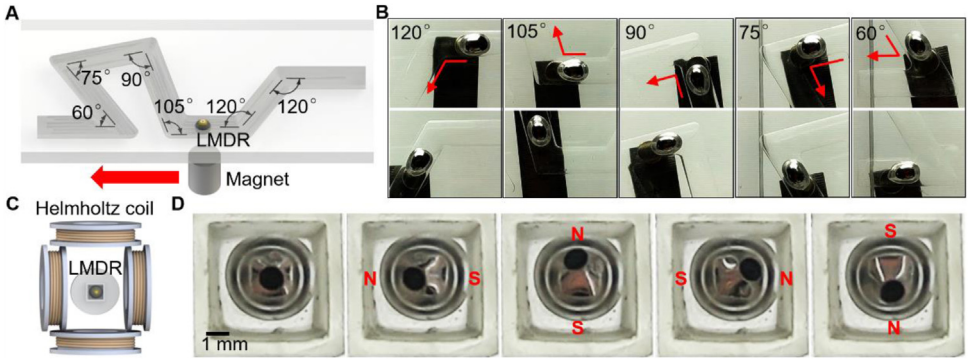

Fig. 3. Investigating the magnetic actuating performance of the LMDR. (A) Schematic of the crooked channel with a varies of angles. (B) Snapshots of controlling the LMDR to pass through different angles. (C) Schematic of the biaxial Helmholtz coil. (D) Sequential snapshots for posture maneuver of the LMDR.

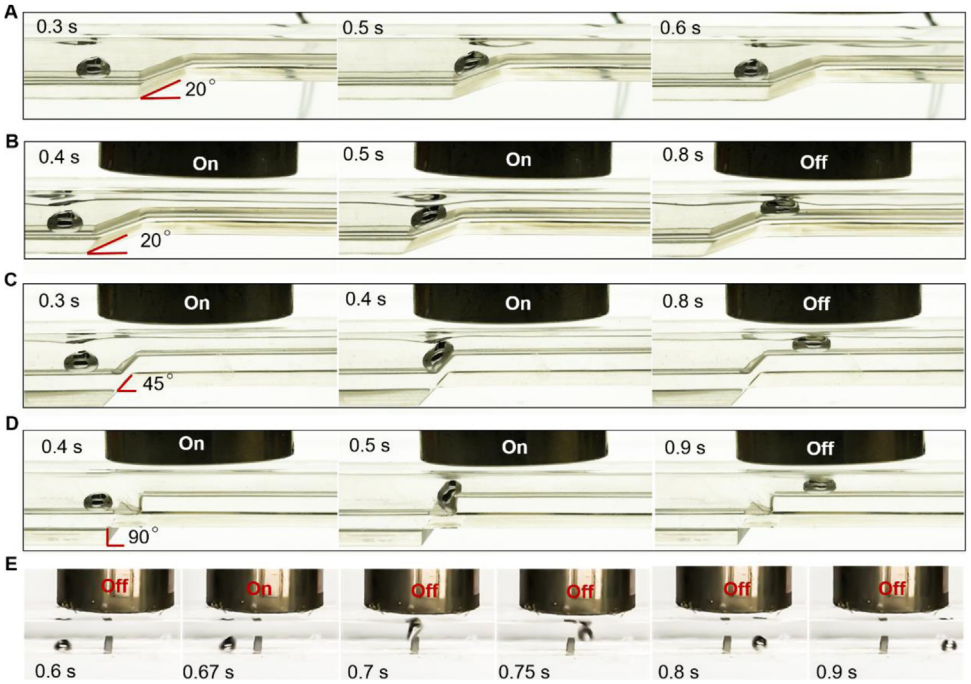

Fig. 4. Maneuvers of the LMDR in 3D space using the interplay of both of electric and magnetic fields. (A) The LMDR failed to climb up the slope with an angle 20°. (B-D) Climbing locomotion of the LMDR on slopes with different angles of 20°, 45° and 90°, respectively. (E) Snapshots showing the obstacle avoidance maneuver of a LMDR.

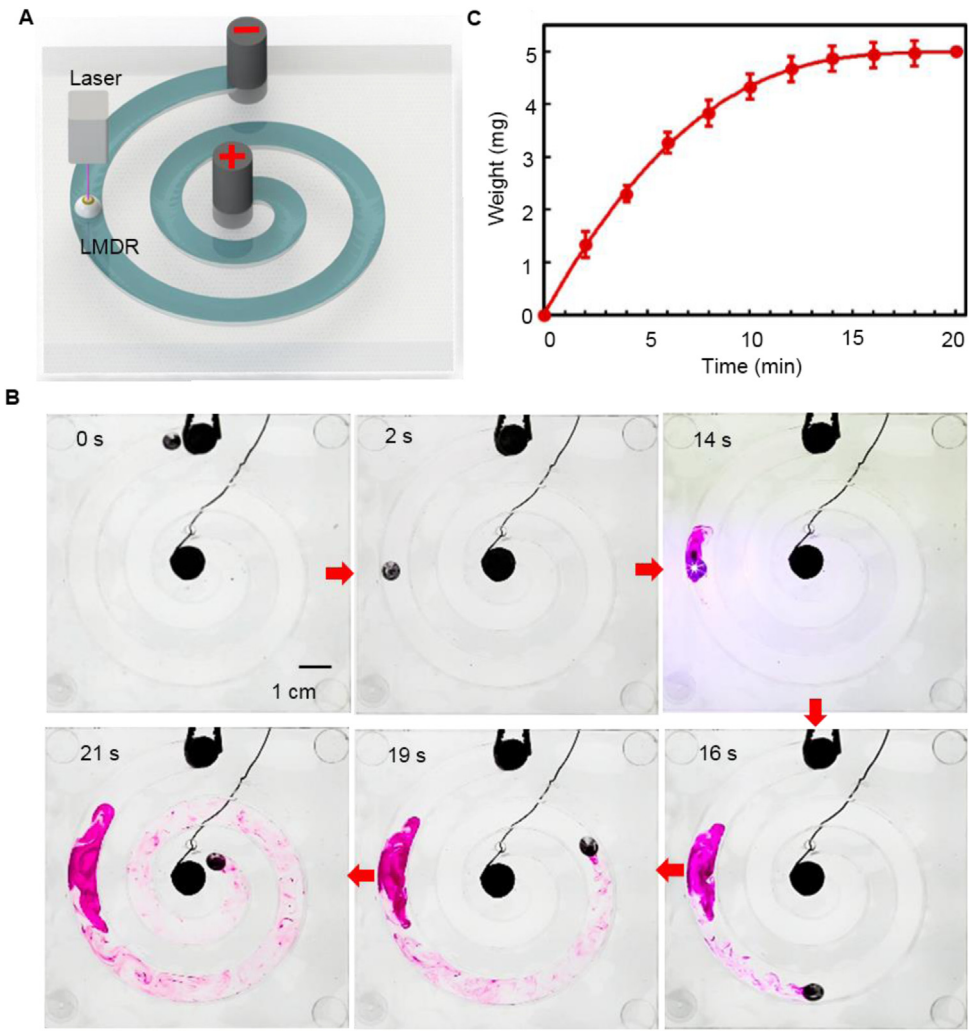

Fig. 5. Controlled chemical delivery and release using the LMDR. (A) Schematic of the experimental setup. (B) Snapshots of the chemical delivery and release process using the LMDR. (C) Release profile of the Phenolphthalein powder in the LMDR.

volume of 100 u L gives the highest speed when the applied voltage is larger than 12 V.

To investigate the position of the IF during electrical actuation, we sealed the IF with purple and white silica gel to indicate its posture in LM droplet. Firstly, we fixed a LMDR in a straight channel filled with NaOH solution and added some orange phosphor powder into the NaOH solution as the indictor to predict the flow patterns. When applying 5 V DC voltage, we observed the formation of two small vortices near the top hemisphere of the LMDR, as shown in Fig. 2E. Meanwhile, the IF always locates on the top of the LMDR without changing its position (Fig. 2E). Next, we released the LMDR to allow it to actuate towards the anode. The suspended particles in the NaOH solution indicates that the surrounding liquid bypassed the IF, and the position and posture of the IF keep unchanged during motion, as shown in Fig. 2F and Movie S1, Supplementary Information.

After understanding the electrical actuating behaviors of the LMDR, we further investigated the control of the LMDR using magnetic field in a crooked channel. The crooked channel has turns with different angles ranging from 45° to 120° and is filled with NaOH solution. A LMDR consists of 250 μL of LM droplet and an IF (60 mg) was used in the experiment. A magnet (B = ~3500 Gs) was placed under the bottom of channel to actuate the LMDR, as shown in Fig. 3A. We can see that the LMDR can smoothly pass through all the turns and exhibits a good deformability in limited space, as shown in Fig. 3B and Movie S2, Supplementary Information.

We further examined the manipulation of the posture of a LMDR using controlled magnetic fields generated by two pairs of biaxial Helmholtz coils (B = ~450 Gs), as shown in Fig. 3C. In doing so, instead of using ferro-magnetic nanoparticles, we sealed a small block of NdFeB permanent magnet (B = ~1200 Gs) in the *driving cabin*. The control performance is illustrated in Fig. 3D, in which we can see that the posture of the IF in the LMDR can be manipulated by controlling the direction of the magnetic field (see Movie S3, Supplementary Information).

After understanding the electrical and magnetic control of the LMDR, we then explored the maneuver of the LMDR in 3D space using the interplay of electric and magnetic fields. This is demonstrated by examining the climbing locomotion of a LMDR in channels with slopes of different angles (height of 3 mm, and angle of 20°, 45° and 90°, respectively). We filled the channel with NaOH (0.5 M) solution and inserted two electrodes at the ends of the channel to provide electrical actuating force for the LMDR along the horizontal direction. Meanwhile, an electromagnet was fixed above the slope to provide an additional magnetic force on the LMDR along the vertical direction. The schematics and actual image of

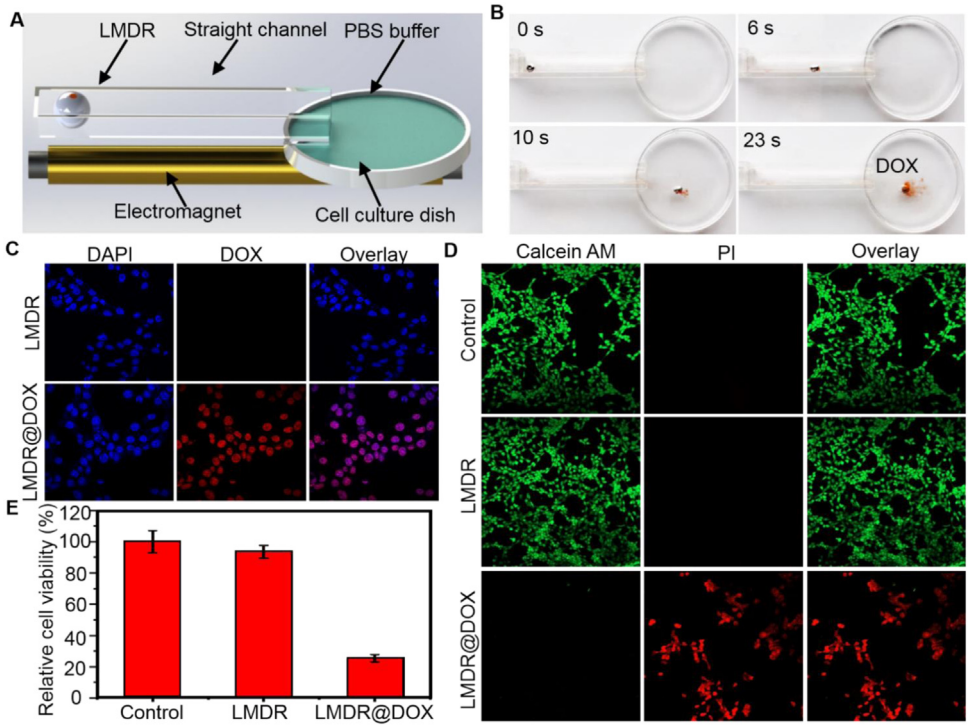

Fig. 6. Targeted drug delivery and therapy trial using the LMDR. (A) Experimental setup. (B) Targeted drug delivery process with a magnetically actuated LMDR. (C) Confocal fluorescence images of LMDR@DOX group and the LMDR group after two hours of incubation. Red and blue colors represent DOX fluorescence and DAPI stained cell nuclei, respectively. (D) Confocal fluorescence images of the LMDR@DOX group, the LMDR group and the control group after 24 h of incubation. The live and dead 4T1 cancer cells were stained with green (Calcein AM) and red (PI) fluorescent dyes, respectively. (E) Viabilities of cells in the LMDR@DOX group, the LMDR group and the control group after 24 h of incubation.

the experimental setup are given in Fig. S3A, Supplementary Information S5. It should be noted that the LMDR is not able to climb up the slope with an angle larger than 20° by its inertia induced by the electrical actuating method (applied DC voltage of 30 V), as shown in Fig. 4A. However, with the interplay of both magnetic (B = ~400 Gs) and electric fields (applied DC voltage of 30 V), the LMDR can successfully climb up slopes even with a steep angle of 90°, as shown in Fig. 4B-D (also see Movie S4 and Supplementary Information S5).

We also found that once the magnetic force exerted on the LMDR is large enough to overcome the gravity of the LMDR, the LMDR is able to leave the substrate and jump in the vertical direction. To demonstrate this, we placed an obstacle (length of 2 mm and height of 3 mm) in the middle of the channel. The schematics and actual image of the experimental setup are given in Fig. S4A, Supplementary Information S6. Upon the application of a 30 V DC voltage to the electrodes and meanwhile activating the electromagnet for 30 ms, we successfully achieved the obstacle avoidance maneuver for the LMDR, as shown in Fig. 4E, (also see Movie S5, Supplementary Information). The dynamics and jump conditions are analysed theoretically in Supplementary Information S6. Also, the jumping height of the LMDRs was characterized by applying magnetic fields with different intensities, as given in Supplementary Information S6.

We designed a proof-of-concept experiment to demonstrate the potential applications of the LMDR in tasks for controlled chemical delivery and release. We filled the cargo cabin of a LMDR (100 μL of LM and 60 mg of IF) with phenolphthalein powder and used it as the indicator of chemical delivery and release processes; we sealed the IF with wax and placed the LMDR into a spiral channel (width of 10 mm, and height of 10 mm) filled with NaOH solution. Two electrodes were fixed at the two ends of the channel to provide the electrical actuating force for the LMDR, and a laser heater was fixed above the channel and aimed at the release position (see Fig. 5A). The chemical delivery and release process of a LMDR is shown in Fig. 5B: *1)* controlled actuation of the LMDR towards the release position was achieved upon the application of DC voltage to the electrodes; *2)* the laser was activated to melt the sealing wax of IF within the LMDR and release the phenolphthalein indicator in the cargo cabin, phenolphthalein powder can quickly react with NaOH solution and make the solution appears to be red; *3)* after further actuating the LMDR along the channel, the red trajectory generated by the phenolphthalein indicator shows that the loaded chemical can be successfully released (also see Movie S6, Supplementary Information). The release profile of the loaded phenolphthalein was quantitatively calibrated. The LMDR was loaded with 5 mg of phenolphthalein powder and placed in a clean Petri dish filled with NaOH solution. We took out the LMDR at different time and measured the weight loss of the LMDR to obtain the release profile, as shown in Fig. 5C. This experiment was repeated using thirty LMDRs. We found that almost all the phenolphthalein powder can be released into the electrolyte solution within 20 min.

Finally, we performed an *in vitro* targeted drug delivery trial to treat cancer cells with a drug loaded LMDR to show the potentials of using the LMDR in developing future targeted drug delivery and therapy system. The design of the *in vitro* targeted drug delivery system is shown in Fig. 6A. The LMDR was loaded with 3.5 mg doxorubicin (DOX) powder and was initially placed at the left end of the straight channel. The right end of the channel was connected to a cell culture dish containing adherent breast cancer (4T1) cells and filled with phosphate buffer solution (PBS). An electromagnet

(B = ~3000 Gs) was placed under the straight channel. The targeted drug delivery process is shown in Fig. 6B. By activating the electromagnet, the LMDR was actuated towards the cell culture dish and immersed into the PBS solution. After 10 s, the color of the PBS solution near the opening of the IF turns red, which indicates that the DOX has been successfully released.

To demonstrate the efficacy of the drug therapy using the LMDR, we prepared three sample groups. The LMDR@DOX group aims to demonstrate the activity of the loaded DOX after releasing from the LMDR, which was prepared by driving and releasing the DOX loaded LMDR into the cell culture dish and then incubated the LMDR with cancer cells together. The LMDR group aims to examine the toxicity of the LMDR and was prepared without loading DOX. For comparison, we also prepared a control group by culturing only the cancer cells without the LMDR. After 2 h of incubation, we took the samples from the LMDR@DOX group and the LMDR group and treated them with DAPI dye [25]. The confocal fluorescence images of the two groups of cells are shown in Fig. 6C, where the blue color denotes the distribution of 4T1 cancer cells, and the red color indicates the distribution of DOX. Only the LMDR@DOX group show a strong DOX fluorescence signal inside the 4T1 cancer cells, indicating the efficient cellular uptake of DOX released from the LMDR [25].

After 24 h of incubation, we treated the cells with Calcein AM/propidium iodide (PI) double staining. The confocal fluorescence images of the cells for the three groups of experiments are shown in Fig. 6D, where live and dead 4T1 cancer cells were stained with green and red colors, respectively. Meanwhile, we also used the Methyl thiazolyl tetrazolium (MTT) assay to evaluate the cell viability of the three groups, as shown in Fig. 6E. It was found that the LMDR does not affect the viability of cells compared with the control group, and most of the cancer cells in the LMDR@DOX group became nonviable after treating with DOX released by the LMDR. These results demonstrate that the proposed LMDR exhibits low cytotoxicity and high targeted drug delivery efficiency in biomedical applications.

4. Conclusion

In this work, we proposed an innovative composite LMDR fabricated by engulfing a functional spherical IF into a LM droplet; this entrusts LM droplets with actuating and enhanced cargo-carrying capability *per se* without destroying the intrinsic properties of LM. The IF can be assembled to or disassembled from the LM droplet using an external electric or magnetic field. We showed that the LMDR appear as a LM droplet but can exhibit an extraordinary actuating performance in 3D space using the interplay of electric and magnetic fields. Such a capability was demonstrated by controlling the LMDRs to climb steep slopes, jump to avoid obstacles, and rotate its body to the desired postures.

Moreover, a proof-of-concept experiment of the controlled transportation and release of chemicals loaded in a LMDR is also performed. Therefore, we showed that the proposed LMDR exhibits a significant improvement in 3D maneuver performance and cargo carrying capability in comparison to bare LM droplets. More importantly, the demonstrated *in vitro* treatment of cancer cells with a DOX loaded LMDR reveals a great potential of developing future targeted drug delivery and therapy system using the LMDR-based platforms.

Declaration of competing interest

The authors declare no competing financial interests

Credit author statements

X. L., S.-Y.T. and S. Z. proposed the project. F. L. and J. S. designed the experiments. F. L., L. Z. and N. Y. performed the experiments. F. L., J. S., L. Z., J. X., S. K., L. C., X. L., S.-Y.T. and S. Z. analysed the results. All authors participated in writing the manuscript.

Acknowledgments

This work is supported in part by grants from the National Natural Science Foundation of China under Grant Nos. 61703294, 61873339, 61503270, 51828503, a grant from National Science Foundation of Jiangsu Province under Grant No. BK20170342, BK20190096, a grant from China Postdoctoral Science Foundation under Grant No. 2016M590497, and supported by the State Key Laboratory of Applied Optics. Dr. Shi-Yang Tang is the recipient of the Vice-Chancellor's Postdoctoral Research Fellowship funded by the University of Wollongong.

Appendix A. Supplementary data

Supplementary material related to this article can be found, in the online version, at doi:https://doi.org/10.1016/j.apmt.2020.100597.

References

[1] N.J. Cira, A. Benusiglio, M. Prakash, Vapour-mediated sensing and motility in two-component droplets, Nature 519 (2015) 446–450.
[2] A. Bouillant, T. Mouterde, P. Bourrianne, A. Lagarde, C. Clanet, D. Quéré, Leidenfrost wheels, Nat. Phys. 14 (2018) 1188–1192.
[3] J. Čejková, T. Banno, M.M. Hanczyc, F. Štěpánek, Droplets as liquid robots, Artif. Life 23 (2017) 528.
[4] T. Liu, P. Sen, C.-J. Kim, Characterization of nontoxic liquid-metal alloy galinstan for applications in microdevices, J. Microelectromechanical Syst. 21 (2012) 443–450.
[5] T. Daeneke, K. Khoshmanesh, N. Mahmood, I.A. de Castro, Liquid metals: fundamentals and applications in chemistry, Chem. Soc. Rev. 47 (2018) 4073–4111.
[6] G. Yun, S.Y. Tang, S. Sun, D. Yuan, Q. Zhao, L. Deng, S. Yan, H.P. Du, M.D. Dickey, Liquid metal-filled magnetorheological elastomer with positive piezoconductivity, Nat. Commun. 10 (2019) 1300.
[7] J. Wissman, M.D. Dickey, C. Majidi, Field-controlled electrical switch with liquid metal, Adv. Sci. 4 (2017), 1700169.
[8] J. Zhang, Y. Yao, L. Sheng, J. Liu, Self-fueled biomimetic liquid metal mollusk, Adv. Mater. 27 (2015) 2648–2655.
[9] T.J. Tang, X. Zhao, J. Li, Y. Zhou, J. Liu, Liquid metal phagocytosis: intermetallic wetting induced particle internalization, Adv. Sci. 4 (2017), 1700024.
[10] S.-Y. Tang, V. Sivan, K. Khoshmanesh, A.P. O'Mullane, X. Tang, B. Gol, N. Eshtiaghi, F. Lieder, P. Petersen, A. Mitchell, K. Kalantar-zadeh, Electrochemically induced actuation of liquid metal marbles, Nanoscale 5 (2013) 5949–5957.
[11] F.X. Li, S.L. Kuang, X.P. Li, J. Shu, W.H. Li, S.Y. Tang, S.W. Zhang, Magnetically- and electrically-controllable functional liquid metal droplets, Adv. Mater. Technol. 4 (2019), 1800694.
[12] M. Li, M.A. Hisham, Y.X. Zhang, S.-Y. Tang, W.H. Li, Automatic morphology control of liquid metal using a combined electrochemical and feedback control approach, Micromachines 10 (2019) 209.
[13] M.R. Khan, C.B. Eaker, E.F. Bowden, M.D. Dickey, Giant and switchable surface activity of liquid metal via surface oxidation, Proc. Natl. Acad. Sci. 111 (2014) 14047–14051.
[14] S.-Y. Tang, V. Sivan, P. Petersen, W. Zhang, P.D. Morrison, K. Kalantar-zadeh, A. Mitchell, K. Khoshmanesh, Liquid metal actuator for inducing chaotic advection, Adv. Funct. Mater. 24 (2014) 5851–5858.
[15] J. Shu, S.-Y. Tang, Z.H. Feng, W.H. Li, X.P. Li, S.W. Zhang, Unconventional locomotion of liquid metal droplets driven by magnetic fields, Soft Matter 14 (2018) 7113–7118.
[16] J. Jeon, J.B. Lee, S.K. Chung, D. Kim, On-demand magnetic manipulation of liquid metal in microfluidic channels for electrical switching applications, Lab Chip 17 (2016) 128–133.
[17] A. Zavabeti, T. Daeneke, A.F. Chrimes, A.P. O'Mullane, O.J. Zhen, A. Mitchell, K. Khoshmanesh, K. Kalantar-zadeh, Ionic imbalance induced self-propulsion of liquid metals, Nat. Commun. 7 (2016) 12402.
[18] X. Tang, S.-Y. Tang, V. Sivan, K. Khoshmanesh, Photochemically induced motion of liquid metal marbles, Appl. Phys. Lett. 103 (2013) 8432.
[19] H. Liu, M. Li, Y. Li, H. Yang, A. Li, T.J. Lu, F. Li, F. Xu, Magnetic steering of liquid metal mobiles, Soft Matter 14 (2018) 3236–3245.

[20] Y. Lu, Q. Hu, Y. Lin, D.B. Pacardo, C. Wang, W. Sun, F.S. Ligler, M.D. Dickey, Z. Gu, Transformable liquid-metal nanomedicine, Nat. Commun. 6 (2015) 10066.
[21] S.A. Chechetka, Y. Yu, X. Zhen, M. Pramanik, K. Pu, E. Miyako, Light-driven liquid metal nanotransformers for biomedical theranostics, Nat. Commun. 8 (2017) 15432.
[22] X.X. Li, J. Xie, S.-Y. Tang, R. Xu, X.P. Li, W.H. Li, S.W. Zhang, A controllable untethered vehicle driven by electrically actuated liquid metal droplets, IEEE Trans. Industr. Inform. 7 (2018) 1.
[23] J. Wu, S.-Y. Tang, T. Fang, W.H. Li, X.P. Li, S.W. Zhang, Wheeled robot driven by liquid metal droplet, Adv. Mater. 30 (2018), 1805039.
[24] L. Sheng, J. Zhang, J. Liu, Diverse transformations of liquid metals between different morphologies, Adv. Mater. 26 (2014) 6036–6042.
[25] L. Cheng, K. Yang, Y. Li, J. Chen, C. Wang, M. Shao, S.T. Lee, Z. Liu, Facile preparation of multifunctional upconversion nanoprobes for multimodal imaging and dualtargeted photothermal therapy, Angew. Chem Int. Ed. 50 (2011) 7385–7390.